Chinese Journal of Electronics
vol. 33, no. 4, pp. 1104–1116, July 2024
https://doi.org/10.23919/cje.2022.00.340

RESEARCH ARTICLE

Cellular V2X-Based Integrated Sensing and Communication System: Feasibility and Performance Analysis

Yibo LI, Junhui ZHAO, Jieyu LIAO, and Fajin HU

School of Electronic and Information Engineering, Beijing Jiaotong University, Beijing 100044, China

Corresponding author: Junhui ZHAO, Email: junhuizhao@hotmail.com
Manuscript Received October 4, 2022; Accepted April 26, 2023

Abstract — Communication and sensing are basically required in intelligent transportation. The combination of two functions can provide a viable way in alleviating concerns about resource limitations. To achieve this, we propose an integrated sensing and communication (ISAC) system based on cellular vehicle-to-everything (C-V2X). We first analyze the feasibility of new radio (NR) waveform for ISAC system. We discuss the possibility of reusing NR waveform for sensing based on current NR-V2X standards. Ambiguity function is calculated to investigate the sensing performance limitation of NR waveform. A C-V2X-based ISAC system is then designed to realize the two tasks in vehicular network simultaneously. We formulate an integrated framework of vehicular communication and automotive sensing using the already-existing NR-V2X network. Based on the proposed ISAC framework, we develop a receiver algorithm for target detection/estimation and communication with minor modifications. We evaluate the performance of the proposed ISAC system with communication throughput, detection probability, and range/velocity estimation accuracy. Simulations show that the proposed system achieves high reliability communication with 99.9999% throughput and high accuracy sensing with errors below 1 m and 1 m/s in vehicle scenarios.

Keywords — Cellular vehicle-to-everything, Integrated sensing and communication, Performance analysis, New radio vehicle-to-everything.

Citation — Yibo LI, Junhui ZHAO, Jieyu LIAO, *et al.*, "Cellular V2X-Based Integrated Sensing and Communication System: Feasibility and Performance Analysis," *Chinese Journal of Electronics*, vol. 33, no. 4, pp. 1104–1116, 2024. doi: 10.23919/cje.2022.00.340.

I. Introduction

The functionalities of both data transmission and environment sensing are crucial in the realm of intelligent transportation [1]. Nowadays, the employment of automotive radar has become a popular means of achieving sensing capabilities [2]. Such technology utilizes radio signals to provide high-resolution sensing for automotive applications such as collision warning. However, specialized equipment needs to be mounted in vehicle and certain frequency bands need be set aside for the provision of sensing service. As for data transmission, vehicle-to-everything (V2X) network makes it possible to communicate in transportation systems [3]. This network facilitates the exchange of safety messages and entertainment information for vehicle services such as localization-based service. Nevertheless, a limited amount of sensing functionality is provided by such V2X network on the basis of raw sensor data and channel measurement. With the view of above challenge, integrated sensing and communication (ISAC) system can be employed for the next generation V2X network.

Various vehicular communication standards have been developed, mostly focusing on dedicated short-range communication (DSRC) and cellular V2X (C-V2X). DSRC, utilizes short-range wireless transmission for vehicle-to-vehicle and vehicle-to-road communication [4]. Additionally, C-V2X is designed for vehicular communication with cellular (Uu) and sidelink communication combined [5], making it suitable for diverse applications. Compared with DSRC, lots of studies have demonstrated C-V2X superiority in aspects such as low latency, high reliability, large transmission range, and high throughput [6]. Therefore, that will be a wise choice to

Guest Editor: Prof. Dongming WANG, Southeast University.

realize ISAC system for vehicles based on C-V2X (i.e., new radio (NR)-V2X), which can reuse existing infrastructure and share available spectrum resource.

The selection of waveform plays a key role in ISAC system. There are some research about waveform design for ISAC system. Some loosely coupled designs can be actualized over temporal domains by non-overlapping wireless resource division [7], which cannot enable communication and sensing simultaneously. Other orthogonal wireless resource designs are implemented in spectral [8] or spatial domains [9], suffering from low spectral and energy efficiency, which can be overcome by a fully integrated waveform design [10]. Despite with the best performance, such a design may have difficulty in deploying to current C-V2X equipment. Therefore, to fill up the implementation gap, it is necessary to analyze the existing waveform for ISAC system. The existing communication waveform has mature signal transceiver with flawless processing performance for communication purpose. Especially, orthogonal frequency division multiplexing (OFDM) waveform, such as NR waveform, has been designed with adaptive modulation across subcarrier, strong robustness against multipath fading, as well as high extensibility in radio system design and resource management [11]. Such features are well-suited for vehicular communication scenarios. It can also be considered as a suitable candidate waveform for use in sensing. Therefore, the communication waveform based on C-V2X is investigated for ISAC system in this paper.

To implement ISAC system by leveraging C-V2X infrastructures, receiver is required to decode information from communication signal and to detect/estimate targets from echoes concurrently [12]. However, communication networks, such as V2X networks, are primarily designed for communication function only [13], which lack the ability to process information for target detection/estimation. To complete the sensing function with communication waveform, specialized received signal processing methods need to be developed. It is possible to learn from the idea of passive radar system used for detection task as a model for ISAC receiver. Such systems have been researched employing typical communication system, including frequency modulation (FM) system [14], digital audio broadcasting (DAB) system [15], digital video broadcasting (DVB) terrestrial transmitters [16], DVB satellite system [17], global system for mobile communications (GSM) base stations [18], Wi-Fi networks [19], and global navigation satellite system (GNSS) [20]. Additionally, a passive radar system has been designed using long term evolution (LTE) network downlink reference signals (RS) and synchronization signals (SS) in [21]. A 5G NR waveform-based OFDM radar has been investigated in [22]. As for vehicular scenarios, IEEE 802.11ad-based system has been proposed for communication and sensing in [23].

In this paper, we propose an ISAC system based on C-V2X network, with NR waveform considered. The main contributions of this paper are as follows.

a) We investigate the sensing performance of NR waveform. First, we overview the NR waveform based on NR-V2X standard and then such waveform is leveraged for ambiguity analysis;

b) An ISAC system based on C-V2X network is proposed. Communication and sensing links are modeled with signal description in detail. Special limitations such as the velocity and distance range of vehicle and the requirement of vehicular network are considered in this research;

c) Receiver signal processing algorithm is developed for communication and sensing. Particularly, communication processing leverages standard time-frequency (TF) synchronization and channel estimation techniques. After communication preprocessing, target detection and range/velocity estimation are realized with periodogram and multiple signal classification (MUSIC) method;

d) Simulations are carried out to evaluate the performance of the proposed ISAC system in C-V2X network. In particular, the proposed ISAC system can achieve m-level range and m/s-level velocity estimation for sensing and reliable throughput for communication;

The rest of the paper is organized as follows: In Section II, standard-based NR waveform sensing performance is analyzed by ambiguity function. System model is described in Section III. Then, receiver processing for communication and sensing is developed in Section IV. Section V evaluates the performance of proposed ISAC system. Section VI concludes the work.

II. NR Waveform Analysis

As the second section of C-V2X technology, NR-V2X has completed standardization work [24]. In this section, we overview the waveform structure of NR-V2X and analyze ambiguity function to assess it suitability as an ISAC waveform for vehicular scenarios.

1. NR-V2X waveform

NR standard's flexible signal strategies offer opportunities for both communication and sensing usage [25]. In NR waveform, to support different application scenarios and enable flexible deployment, variable cyclic prefix (CP) duration and scalable subcarrier spacing (SCS) are defined in frequency range 1 (FR1) and frequency range 2 (FR2) [26]. OFDM waveform numerology $\mu = \{0, 1, \ldots, 4\}$ plays a key role in the design of SCS and CP. Specifically, SCS is defined as a superset of 15 kHz, denoted by $\Delta f^{\mu} = 2^{\mu} \times 15$ kHz. For FR1, $\mu = 0, 1, 2$ are used, corresponding to 15 kHz/30 kHz/60 kHz SCS and up to 100 MHz single carrier bandwidth. $\mu = 3, 4$ are used in FR2 with 120 kHz/240 kHz SCS and up to 400 MHz single carrier bandwidth. These parameters have influence on the performance of communication and sensing.

For NR-V2X, TF resource element (RE) is allocated in both NR Uu and sidelinks [27]. Specifically, the

subframe includes some timeslots depending on μ. Each timeslot involves 14 OFDM symbols with normal CP (nCP) or 12 symbols with extended CP (eCP), which determines the duration of symbols T. So M-length complex baseband OFDM waveform with N subcarriers is,

$$x(t)=\sum_{m=0}^{M-1}\sum_{n=0}^{N^{\mu}-1}x_{m,n}\mathrm{e}^{\mathrm{j}2\pi n\Delta f^{\mu}t}\,\mathrm{rect}\left(\frac{t-N^{\mu}_{\mathrm{sym},m}T_c}{N^{\mu}_{\mathrm{sym},m}T_c}\right) \quad (1)$$

where $x_{m,n}$ is the transmitted symbol sequence corresponding to RE; OFDM basic time unit is $T_c=\frac{1}{\Delta f^{\mu}_{\min}N_{\mathrm{FFT}}}$, where N_{FFT} is the size of fast Fourier transform (FFT) matrix; and symbol duration with CP is, $N^{\mu}_{\mathrm{sym},m}T_c=N^{\mu}_{\mathrm{cp},m}T_c+N^{\mu}_{\mathrm{s},m}T_c$, where $N^{\mu}_{\mathrm{s},m}=(m-1)\times 2^{-\mu+11}$ is non-CP symbol duration.

To get better matched filter gain, using an OFDM waveform with pseudo-random code provides a better self-correlation performance than that without code, which is beneficial for sensing processing. As for NR-V2X, both Uu and sidelink (PC5) interfaces support SS and RS [28], which are suitable for sensing task. In NR downlink transmission, sidelink primary-SS and sidelink secondary-SS are collected to construct SS block. Phase tracking-RS (PT-RS), channel state information-RS (CSI-RS), and demodulation-RS (DM-RS) are used to construct RS block. These signals are viewed as "constantly available", which can be utilized for conveying sensing information. Besides, physical broadcast channel, including physical sidelink broadcast channel (PSBCH) in sidelinks and physical downlink shared channel (PDSCH) in Uu links, is used for the transmission of data payload and hyper-layer signal, which carry communication and sensing information. Another benefit is that the deployment of SS and RS blocks can be adjusted in TF domain via hyper-layer parameters.

2. Ambiguity function analysis

We employ the ambiguity function to evaluate the feasibility of NR-V2X waveform for sensing [29] as

$$A(\tau,f_d)=\frac{1}{E_x}\left|\int_{-\infty}^{\infty}x(t)x^*(t-\tau)\mathrm{e}^{\mathrm{j}2\pi f_d t}\mathrm{d}t\right| \quad (2)$$

where E_x is the squared norm of the signal, calculated as $E_x=\int_{-\infty}^{\infty}x(t)x^*(t)\mathrm{d}t=\sum_{m=0}^{M-1}\sum_{n=0}^{N^{\mu}-1}|x_{m,n}|^2$. $x(t)$ is the NR waveform. τ and f_d are the time delay and Doppler shift, respectively. And x^* denotes the complex conjugate.

To assess the performance of NR-V2X waveform [30], we generate an NR downlink signal based on current standards. Specifically, NR waveform is constructed with $\mu=1$, where the bandwidth of each subcarrier is 30 kHz with nCP. The bandwidth of 20 resource blocks at 30 kHz is 7.2 MHz. We further configure SS and RS blocks with PDSCH as slot-wise mapping type and modulation scheme 16-quadrature amplitude modulation (16QAM). Its TF resource including PDSCH, DM-RS, and PT-RS configuration is mapped as Figure 1.

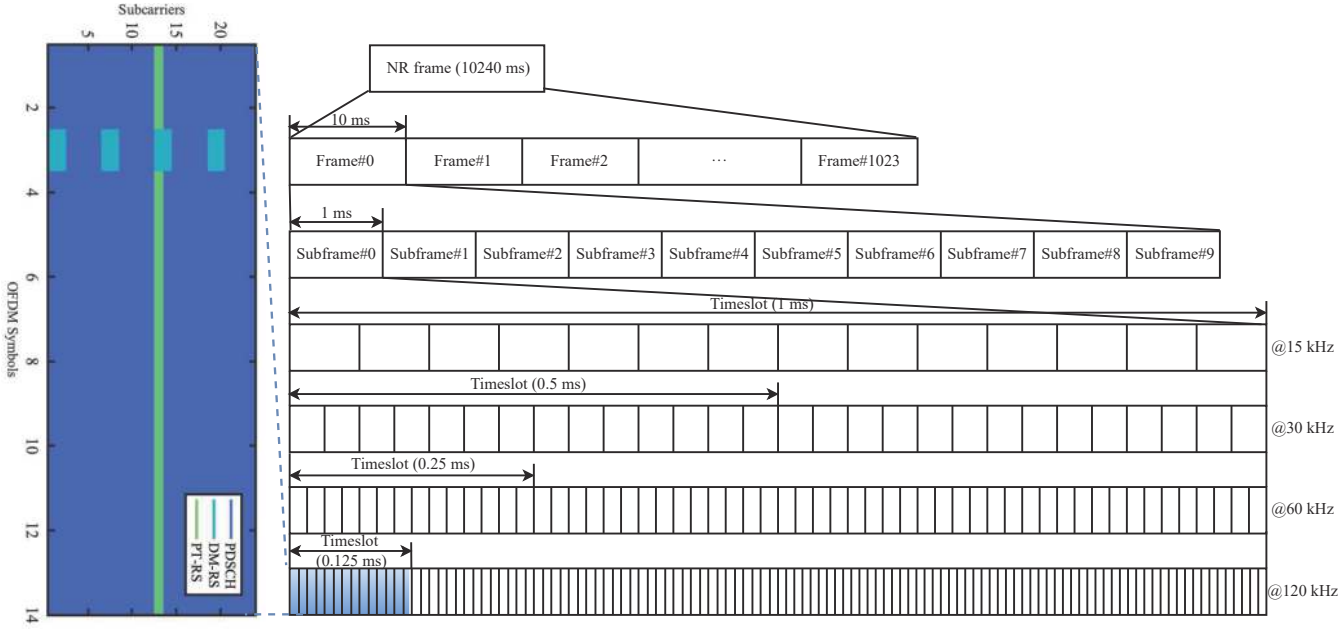

Figure 1 Time-frequency resource grid.

The ambiguity function is shown in Figure 2, which resembles "pin". This shape shows its advantageous correlation properties, which offer a very narrow mainlobe width (leading to high resolution) and an extremely low sidelobe power (deriving to high dynamic range). The zero-Delay cut is depicted in Figure 3, which has a peak time in 0 kHz. This indicates that NR waveform has a perfect auto-correlation with no obvious sidelobe along Doppler axis and strong clutter suppression capability, making it ideal for velocity estimation.

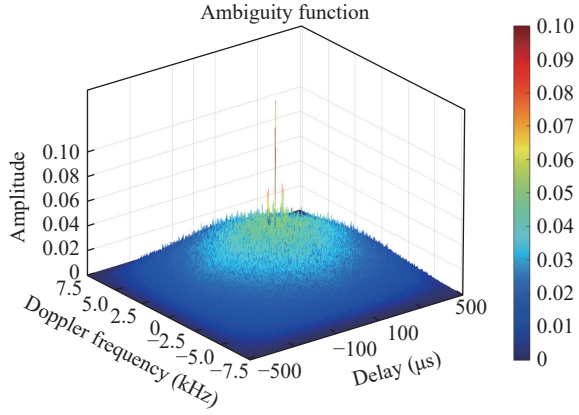

Figure 2 Ambiguity function of NR waveform.

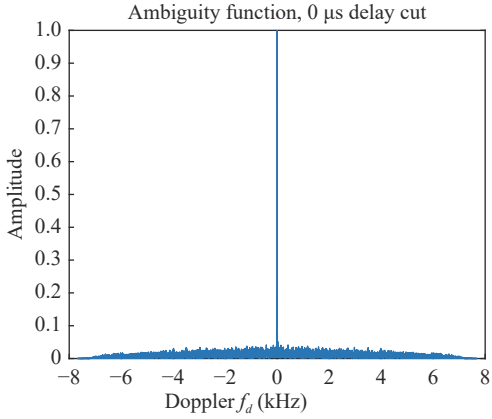

Figure 3 Zero-delay cut of NR waveform ambiguity function.

In Figure 4, we examine delay domain performance by zero-Doppler cut. The second peak locates in 33.34 μs, which is related to the duration of OFDM symbol with SCS 30 kHz. The corresponding sensing range ambiguity is 5 km, which can be ignored for targets in vehicular scenarios. With the above view, standardized NR waveform shows its good sensing performance for multi-target detection/estimation.

III. System Model

In this section, we design the ISAC system based on C-V2X and formulate end-to-end model for the proposed

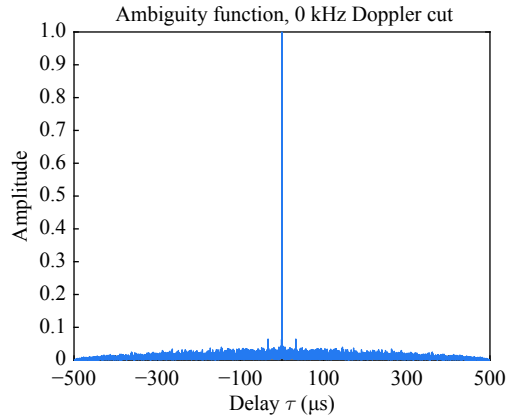

Figure 4 Zero-Doppler cut of NR waveform ambiguity function.

system. The system scenario assumes that every vehicle and road side unit (RSU) serves as an ISAC transceiver. For ease of explanation, we focus on one RSU as ISAC transceiver, which sends an OFDM-based ISAC waveform to a vehicle receiver, and receives echo signal reflected from a single vehicle target, as shown in Figure 5. A multiple-antenna is mounted with N_{Tx}-element transmit antenna array on RSU and N_{Rx}-element receive antenna array on both RSU and vehicle. Furthermore, we assume that the acceleration and the relative velocity of target vehicle to RSU are negligible enough to provide constant velocity and quasi-stationary presumption during one interval. With the above assumption, firstly, a signal model based on OFDM waveform is generated at the RSU, which serves as the transmit signal for communication and sensing functions. Then, we describe one-way communication channel and two-way sensing channel reflected from target in detail. Finally, the received signals are formulated in communication and sensing sides, respectively.

1. ISAC Tx signal

The ISAC waveform is generated based on current waveform design for NR Uu and PC5, which supports OFDM baseband signal uniformly defined by 4-dim tuple (m, n, p, μ), where $m \in \{0, 1, \ldots, M-1\}$ is OFDM symbol index in T-domain, $n \in \{0, 1, \ldots, N^{\mu}-1\}$ is sub-

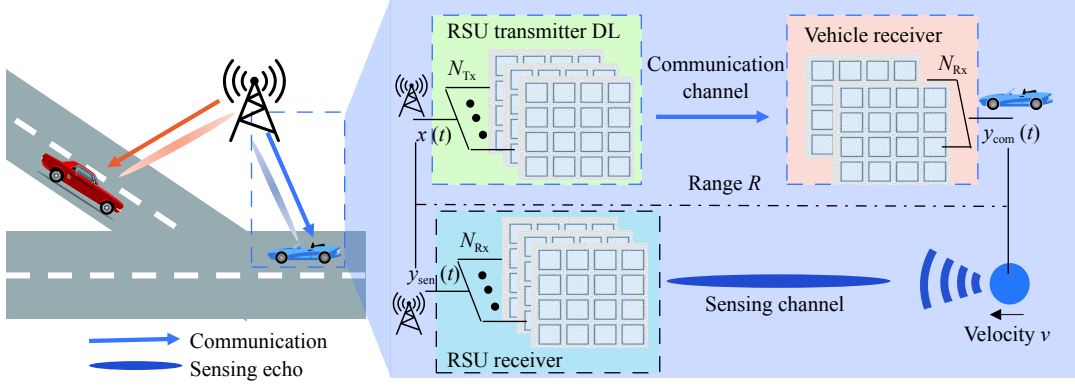

Figure 5 Proposed ISAC system in vehicular network.

carrier index in F-domain, $p = N_{\mathrm{Rx}}$ is antenna port, and μ is SCS configuration parameter, expressed as

$$s^{(p,\mu)}(t) = \sum_{m=0}^{M-1} \sum_{n=0}^{N^{\mu}-1} x_{m,n}^{(p,\mu)} \mathrm{e}^{\mathrm{j}2\pi n \Delta f^{\mu} t} g(t - nT) \tag{3}$$

The carrier configuration is created as the description in Section II. Such frequency domain OFDM symbol is transformed into T-domain by CP-OFDM modulation. To transmit the waveform with multi-antenna, the Tx/Rx frequency-flat analog beamforming vectors $\boldsymbol{A}_{\mathrm{Tx}} \in \mathbb{C}^{N_{\mathrm{Tx}} \times 1}$ into baseband model. Therefore, in the processing interval T_{inv}, the transmitted signal is

$$x_{\mathrm{Tx}}(t) = \boldsymbol{A}_{\mathrm{Tx}} s^{(p,\mu)}(t),\ t \in (0, T_{\mathrm{inv}}) \tag{4}$$

The average power constraint is given by

$$\frac{1}{PNM} \sum_{p=0}^{P-1} \sum_{n=0}^{N-1} \sum_{m=0}^{M-1} \mathbb{E}\left[\left| x_{m,n}^{(p,\mu)} \right|^2 \right] \leq E_{\mathrm{avg}} \tag{5}$$

2. Sensing and communication channel

We build one-way communication and two-way sensing channel model, including the contributions of fading factor, scattering clusters, interference, and clutter. Concretely, fading factor is predominantly determined by fading channel and radar cross section (RCS) of target vehicle. To mitigate self-interference, we utilize a combination of Tx and Rx antenna array separation, self-interference cancellation mechanisms, and beamforming, which provide effective isolation and cancellation for communication and sensing functions. Furthermore, 5G NR medium access control (MAC) protocol is employed to avoid inter-user interference [31]. The clutter arises from the processing of unwanted scatter and clutter cancellation, which is typically treated as noise. We presume that beams transmit without any obstruction. So, the communication and sensing channel is modeled as a dominated line-of-sight (LOS) path between RSU and vehicles. To provide less clutter, lower interference, and longer detection range, narrow beams are utilized with larger beamforming gain. We also assume that beams are wide enough to cover the center of target vehicle and narrow enough to meet the requirements of communication. Therefore, the recipient vehicle is defined as a single point target with distance of r and moving with relative radial velocity of v, RCS of which is 1 m^2. Due to the quasi-stationary assumption, range and velocity are viewed to be constant.

1) Sensing channel

The sensing channel is assumed to be a sum of contributions from direct path scatters. We consider the direct path and corresponding reflected echo signal as two-way channel path. That channel model with K targets is given by

$$h_{\mathrm{sen}}(t, \tau) = \sum_{k=0}^{K-1} h_{\mathrm{sen},k} \delta(\tau - \tau_k) \mathrm{e}^{\mathrm{j}2\pi f_{d,k} t} \tag{6}$$

where τ_k denotes the kth target round-trip delay, $f_{d,k}$ is the Doppler shift, and h_{sen} denotes the channel gain, given by $h_{\mathrm{sen},k} = g_{\mathrm{sen}} G_{\mathrm{sen}}$, where g_{sen} is small-scale complex channel gain. G_{sen} is large-scale channel gain, which is assumed as free-space path-loss model considering target RCS derived by radar equation, $G_k = \frac{\lambda^2 \sigma_{\mathrm{RCS},k}}{(4\pi)^3 r_k^4}$, where $\sigma_{\mathrm{RCS},k}$ is the RCS corresponding to the kth target. We consider a distant target whose r_k is large compared to the distance change of duration T, that is $r_k \gg v_k T$. Therefore, $h_{\mathrm{sen},k}$ is constant during a correlated duration.

It is noted that the round-trip delay τ_k and Doppler shift $f_{d,k}$ corresponding to parameters of the kth target echo are related to its range and velocity,

$$r_k = \frac{\tau_k c}{2},\ \ v_k = \frac{f_{d,k} c}{2 f_c} \tag{7}$$

where c is the speed of light and f_c is the center of frequency. The transfer function is $\Omega(\tau_k, f_{d,k}) = (r_k, v_k)$.

2) Communication channel

Transmit waveform through a clustered delay line (CDL) channel model with delay profile CDL-C. The delay spread and maximum Doppler shift parameter is configured as the 3rd Generation Partnership Project (3GPP) standard [32]. By taking the time frequency selective channel into consideration, the one-way communication channel is given by

$$h_{\mathrm{com}}(t, \tau) = \sum_{k=0}^{K-1} g_{\mathrm{com}} G_{\mathrm{com}} \mathrm{e}^{\mathrm{j}\pi f_{d,k} t} \delta\left(\tau - \frac{\tau_k}{2}\right) \tag{8}$$

where g_{com} and G_{com} denote the small-scale and large-scale communication channel gain, respectively.

3. Receive signal

We consider the communication signal received by recipient vehicle and sensing echo signal received by RSU, with ISAC waveform propagated after the communication channel and sensing channel, respectively.

1) Sensing received signal model

The echo signal received after sensing channel is

$$\begin{aligned} y_{\mathrm{sen}}(t) &= \int h_{\mathrm{sen}}(t, \tau) x_{\mathrm{Tx}}(t - \tau) \mathrm{d}\tau \\ &= \sum_{k=0}^{K-1} h_{\mathrm{sen},k} x_{\mathrm{Tx}}(t - \tau_k) \mathrm{e}^{\mathrm{j}2\pi f_{d,k} t} + n(t) \end{aligned} \tag{9}$$

where $n(t)$ is the sum of contributions from noise and clutter, which is assumed to be an i.i.d complex gain additive white Gaussian noise.

By sampling every T/M and removing the CP, we obtain the discrete-time signal. Then, after discrete Fourier transform (DFT), the received signal correspond-

ing to the mth symbol in the nth SCS is

$$Y_{\text{sen},n,m} = \sum_{k=0}^{K-1} h_{\text{sen},k} \mathrm{e}^{\mathrm{j}2\pi nTf_{d,k}} \mathrm{e}^{-\mathrm{j}2\pi m\Delta f\tau_k} X_{n,m} + N_{n,m} \tag{10}$$

where $N_{n,m}$ is discrete clutter-plus-noise distributed as $\mathcal{N}\left(0,\sigma^2\right)$.

2) Communication received signal model

The communication received by recipient vehicle after propagation channel is

$$\begin{aligned} y_{\text{com}}(t) &= \int h_{\text{com}}(t,\tau) x_{\text{Tx}}(t-\tau)\mathrm{d}\tau \\ &= \sum_{k=0}^{K-1} h_{\text{com},k} x_{\text{Tx}}\left(t-\frac{\tau}{2}\right) \mathrm{e}^{\mathrm{j}\pi f_{d,k}t} + n(t) \end{aligned} \tag{11}$$

After time/frequency synchronization and symbol rate sampling, the discrete-time received communication signal at the recipient vehicle is

$$Y_{\text{com},n,m} = \sum_{k=0}^{K-1} h_{\text{com},k} \mathrm{e}^{\mathrm{j}2\pi nTf_{d,k}} \mathrm{e}^{-\mathrm{j}2\pi m\Delta f\tau_k/2} X_{n,m} + N_{n,m} \tag{12}$$

Signal-to-noise ratio (SNR) of the received communication and sensing signal is defined as average SNR every RE per receive antenna. Because of guard bands or zero padding, signal allocation can occupy only a part of available grids, while noise occupies all REs. Considering these definitions, SNR in RSU and vehicle receiver are respectively given by

$$\text{SNR}_{\text{sen}} = \frac{H_{\text{sen}}^2 \mathbb{E}\left[|x_{m,n}|^2\right]}{N^2} = \frac{\lambda^2 \sigma_{\text{RCS},k} g_{\text{sen}} \mathbb{E}\left[|x_{m,n}|^2\right]}{(4\pi)^3 r_k^4 \sigma^2} \tag{13}$$

$$\text{SNR}_{\text{com}} = \frac{H_{\text{com}}^2 \mathbb{E}\left[|x_{m,n}|^2\right]}{N^2} = \frac{\lambda^2 g_{\text{com}} \mathbb{E}\left[|x_{m,n}|^2\right]}{(4\pi)^2 r_k^2 \sigma^2} \tag{14}$$

where overall received power over all antennas is one.

IV. Receiver Processing

We consider the communication receiver processing in recipient vehicle, which is also applied in the sensing preprocessing in RSU. The sensing receiver processing is then used for target detection and range/velocity estimation step. Such proposed algorithm meets the requirement of ISAC system using conventional C-V2X devices with minimal receiver modifications.

Based on the above signal and system analysis, when performing a sensing task, the algorithm considers two observation scenarios: 1) Mono-static sensing scenarios: NR base station is used as RSU to sense surrounding environment. Therefore, the received echo signal can be processed via known transmitted NR waveform directly. 2) Bi-static sensing scenarios: The transmitter and receiver are separated in RSU. The transmitted signal structure can be predetermined as a prior with SS blocks and we can treat the transmitted waveform as known signal after communication processing. So as for the sensing processing in receiver side, we can process echo signals considering transmitter signal and the influence caused by Tx/Rx.

As is shown in Figure 6, the following processing is exploited to realize communication and sensing functions: 1) Communication: Conventional communication processing is used with TF synchronicity and channel estimation; 2) Detection: After communication preprocessing, target vehicle is detected using a threshold algorithm for constant false alarm rate (CFAR) detector; 3) Estimation: Range/velocity estimation is calculated with periodogram and MUSIC methods.

1. Communication receiver processing

In the vehicle recipient receiver, communication preprocessing is exploited for received signal, which undergoes OFDM demodulation to transform T-domain waveform to F-domain waveform. The resulting demodulation signal $Y_{m,n}$ is used for sensing processing directly, while the module of communication preprocessing is used to abstract $X_{m,n}$. The $X_{m,n}$ is achieved by the following steps [33]:

First, a TF synchronization is performed using a cross-correlation of the received signal with PDSCH DM-RS and PT-RS in T-domain.

Then, channel estimation is carried out to characterize channel effects per RE, with reference symbols used to estimate channel conditions and noise averaging and interpolation to obtain an estimate for all REs in slots. Because such symbols are specified per layer, the result represents channel conditions between transmit layers and receive antennas, which takes into account the effect of MIMO precoding.

Finally, equalization is performed to compensate for distortion introduced by channel.

The PDSCH symbols are extracted from received grids and associated channel estimates. CSI is used as a measure of channel conditions for each of equalized PDSCH symbols. Such CSI information weights decoded soft bits after PDSCH decoding, which effectively increases the importance of symbols experiencing better channel conditions. It is noted that $X_{m,n}$ is known as a prior in such ISAC system. With the view of this, data transmission matrix can also be obtained from transmitters without any calculation of channel estimation and precoding matrix at receiver ends.

The communication preprocessing data subsequently undergoes decoding equalized PDSCH symbols to obtain soft bit codewords [34]. To improve the accuracy of decoding, we scale soft bits or log-likelihood ratios (LLRs) using CSI. This scaling assigns a larger weight to symbols in REs with better channel conditions. LLRs are then decoded using DL-SCH decoding process to check

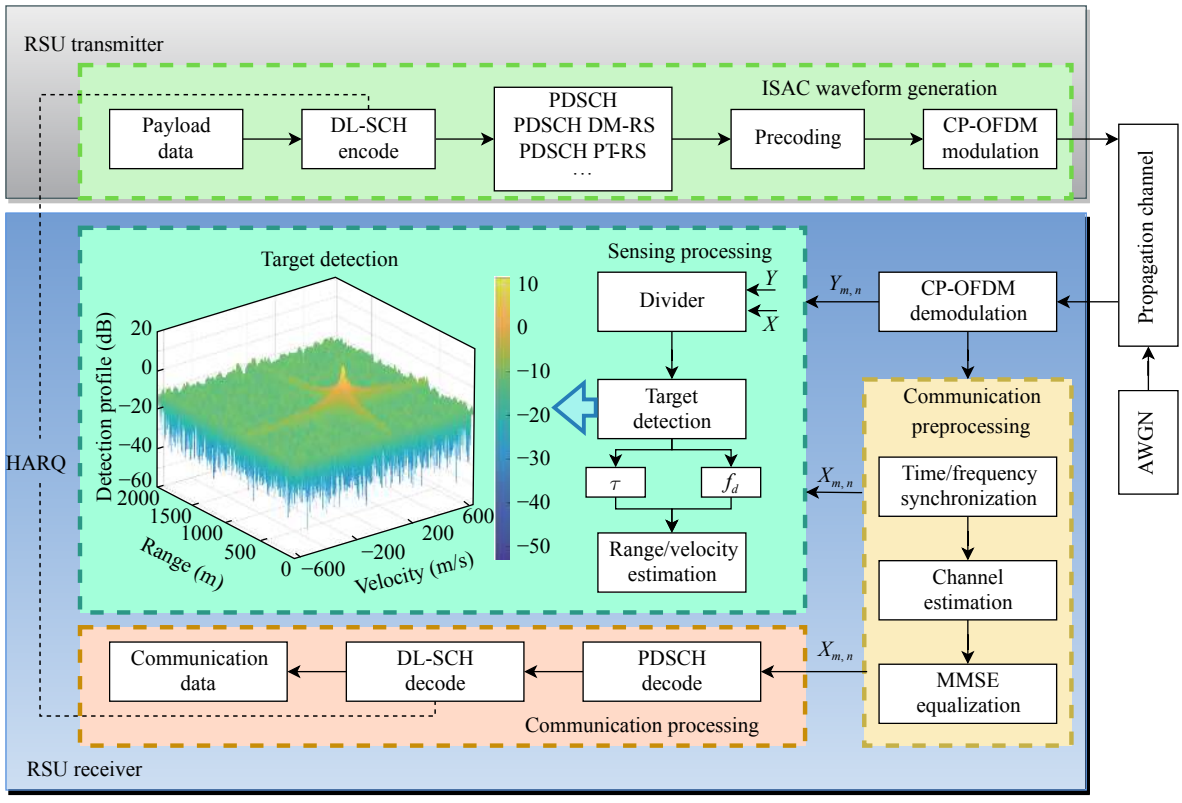

Figure 6 ISAC receiver processing in RSU side.

for errors. In order to enhance throughput, hybrid automatic repeat request (HARQ) management is employed. HARQ manages whether new data is required, which occurs when a transport block is received successfully or if a sequence timeout has occurred. LLRs error status is used to update current HARQ, which is then advanced to the next processing.

2. Target detection

After communication receiver processing, we obtain the known transmitted waveform which is implemented in sensing processing. We utilize directly the known transmitted signal sample $X_{m,n}$ and received signal sample $Y_{m,n}$ after subcarrier-domain processing. The classical matched filtering-based approach is

$$\begin{aligned}\tilde{F}_{m,n} &= Y_{m,n}X^*_{m,n} \\ &= \sum_{k=0}^{K-1} h_{\text{sen}} |X_{m,n}|^2 \, \mathrm{e}^{\mathrm{j}2\pi nTf_{d,k}} \mathrm{e}^{-\mathrm{j}2\pi m\Delta f\tau_k} + \tilde{N}_{m,n}\end{aligned} \tag{15}$$

The analysis of range and velocity profiles reveals their clear dependence on the data. Additionally, matched filter-based processing suffers from range profile sidelobes, thereby limiting its applicability in dynamic scenarios like V2X, as is shown in ambiguity function analysis in Section II. Instead, a data-independent approach can be adopted. We follow channel estimation-based sensing processing, which can be described at OFDM symbol level as

$$F_{m,n} = \frac{Y_{m,n}}{X_{m,n}} = \sum_{k=0}^{K-1} h_{\text{sen}} \mathrm{e}^{\mathrm{j}2\pi nTf_{d,k}} \mathrm{e}^{-\mathrm{j}2\pi m\Delta f\tau_k} + \tilde{N}_{m,n} \tag{16}$$

Only one single target is investigated in this paper, so we assume $K = 1$. The range-Doppler response can be calculated through periodogram, expressed as

$$D(p,q) = \underbrace{\left| \sum_{n=0}^{N_{\text{FFT}}-1} \overbrace{\left(\sum_{m=0}^{M_{\text{FFT}}-1} (W_{m,n} F_{m,n} \mathrm{e}^{-\mathrm{j}2\pi q \frac{m}{M_{\text{FFT}}}} \right)}^{\text{FFT - velocity profiles}} \mathrm{e}^{\mathrm{j}2\pi p \frac{n}{N_{\text{FFT}}}} \right|}_{\text{IFFT - range profiles}} \tag{17}$$

where the values of $N_{\text{FFT}} > N$ and $M_{\text{FFT}} > M$ are chosen to increase the accuracy of detection. CFAR detector is then applied in target detection [29], given by

$$D(p,q) \underset{H_1}{\overset{H_0}{\lessgtr}} T_{\text{th}} \tag{18}$$

where H_0 refers to the null hypothesis (no target, noise only), while H_1 refers to alternative hypothesis (target present). Specifically, the probability of false alarm P_{FA} represents $D(p,q) > T_{\text{th}}$ under H_0 being true. T_{th} is detection threshold, which can be straight calculated to fix P_{FA} to a chosen value. The additional weights $W_{m,n}$ can be set as window function to control sidelobe levels. With CFAR detection and sidelobe mitigation, we can improve the probability of detection.

3. Range/velocity estimation

If threshold test declares that a target is present, the estimation of target range/velocity can be implemented. An estimator is constructed for the case where target is present, and there is no prior information about the target. A parameter vector is $\boldsymbol{\theta} = (\tau, f_d)$.

The likelihood function for $F_{m,n}$ with a given parameter vector [35] is

$$f(\boldsymbol{F} \mid \boldsymbol{\theta}) = \prod_{m=0}^{M-1} \prod_{n=0}^{N-1} \frac{1}{\pi \tilde{\sigma}^2} \mathrm{e}^{-\frac{\left|F_{m,n} - \mathrm{e}^{\mathrm{j}2\pi(nTf_{d,0} - m\Delta f \tau_0)}\right|^2}{\tilde{\sigma}^2_{m,n}}} \tag{19}$$

which is corresponded as log-function, expressed as

$$\ell(\boldsymbol{F} \mid \boldsymbol{\theta}) = \sum_{m=0}^{M-1} \sum_{n=0}^{N-1} \Big(-\log \pi \tilde{\sigma}^2_{m,n} - \frac{1}{\tilde{\sigma}^2_{m,n}} \left| F_{m,n} - \mathrm{e}^{\mathrm{j}2\pi(nTf_{d,0} - m\Delta f \tau_0)} \right|^2 \Big) \tag{20}$$

That function can be simplified with terms ignored, which not affect estimation parameters, that is

$$\tilde{\ell}(\boldsymbol{F} \mid \boldsymbol{\theta}) = \sum_{m=0}^{M-1} \sum_{n=0}^{N-1} \mathrm{Re}\left\{ F_{m,n} \mathrm{e}^{\mathrm{j}2\pi(nTf_{d,0} - m\Delta f \tau_0)} \right\} \tag{21}$$

The maximum likelihood estimation for the target is

$$\hat{\boldsymbol{\theta}} = \arg\max_{\boldsymbol{\theta}} \tilde{\ell}(\boldsymbol{F} \mid \boldsymbol{\theta}) \tag{22}$$

where $\boldsymbol{\theta} \in \Omega_A$, which is related to the $R_{\max}$ and $V_{\max}$.

The above equation is corresponded to the location of periodogram's peak from (19). We can calculate the resolution by transfer function $\Omega(\tau, f_d)$ with basic pixel size of range-Doppler response image Δv and Δr. So range/velocity estimation can be respectively obtained by

$$\hat{r} = \Omega_r \left\{ \frac{1}{M} \sum_{m=0}^{M_{\mathrm{FFT}}-1} \arg\max \left(\sum_{n=0}^{N_{\mathrm{FFT}}-1} F_{m,n} \mathrm{e}^{\mathrm{j}2\pi p \frac{n}{N_{\mathrm{FFT}}}} \right) \right\} \tag{23}$$

$$\hat{v} = \Omega_v \left\{ \frac{1}{N} \sum_{n=0}^{N_{\mathrm{FFT}}-1} \arg\max \left(\sum_{m=0}^{M_{\mathrm{FFT}}-1} F_{m,n} \mathrm{e}^{-\mathrm{j}2\pi q \frac{m}{M_{\mathrm{FFT}}}} \right) \right\} \tag{24}$$

Range/velocity estimation from (25) is viewed as phase estimation. MUSIC algorithm is the most popular method for direction finding [36], which can also be used in sensing estimation in proposed system. Receiver signal processing function is rewritten as

$$\boldsymbol{F} = \sum_{k=0}^{K-1} h_{\mathrm{sen}} \boldsymbol{a}_r(\theta_{\tau,k}) \boldsymbol{a}_{v,k}(\theta_{f_d}) + \tilde{\boldsymbol{N}} \tag{25}$$

where we assume $K = 1$, and $\boldsymbol{a}_r$ is the range phase vector, given by $\boldsymbol{a}_{r,m}(\theta_\tau) = \mathrm{e}^{-\mathrm{j}2\pi m \theta_\tau}$

Then, the covariance matrix is calculated as

$$\boldsymbol{C}_{\boldsymbol{F},r} = \mathbb{E}\left\{ \boldsymbol{F}\boldsymbol{F}^{\mathrm{H}} \right\} = \delta^2 \boldsymbol{a}_r \boldsymbol{a}_r^{\mathrm{H}} + \tilde{\sigma}^2 \boldsymbol{I} \tag{26}$$

where $\mathbb{E}\{\cdot\}$ denotes the expectation operation and δ^2 is variance. Through eigendecomposition, above equation can be rewritten as

$$\boldsymbol{C}_{\boldsymbol{F},r} = \boldsymbol{U}_R \boldsymbol{\Lambda} \boldsymbol{U}_R^{\mathrm{H}} \tag{27}$$

where $\boldsymbol{\Lambda}$ is a diagonal matrix composed of eigenvalues in descending order as $\boldsymbol{\Lambda} = \mathrm{diag}\{\lambda_1, \lambda_2, \ldots, \lambda_M\}$, and $\boldsymbol{U}_R = [\boldsymbol{U}_r \boldsymbol{U}_{\mathrm{noise}}]$ is an M-dim eigenvector matrix whose first column vectors correspond to range estimation subspace by $\boldsymbol{U}_r$, and the remaining $M-1$ column vectors are noise subspace eigenvectors as $\boldsymbol{U}_{\mathrm{noise}} \in \mathbb{C}^{M \times (M-1)}$. Using the orthogonality of target and noise subspaces, and the fact that the columns of $\boldsymbol{U}_r$ and $\boldsymbol{a}_r$ span the same space, we have $\left\| \boldsymbol{U}_{\mathrm{noise}}^{\mathrm{H}} \boldsymbol{a}_r \right\|_{\mathcal{F}} = 0$, where $\mathcal{F}$ is the Frobenious norm. Finally, we obtain the MUSIC spectra of range estimation $P(\theta_\tau)$ as

$$P(\theta_\tau) = \frac{1}{\boldsymbol{a}^{\mathrm{H}}(\theta_\tau) \boldsymbol{U}_{\mathrm{noise}} \boldsymbol{U}_{\mathrm{noise}}^{\mathrm{H}} \boldsymbol{a}(\theta_\tau)} \tag{28}$$

whose largest peaks correspond to target range estimation θ_r. The covariance matrix for velocity estimation can be expressed as

$$\boldsymbol{C}_{\boldsymbol{F},v} = \mathbb{E}\left\{ \boldsymbol{F}^{\mathrm{H}} \boldsymbol{F} \right\} = \delta^2 \boldsymbol{a}_v \boldsymbol{a}_v^{\mathrm{H}} + \tilde{\sigma}^2 \boldsymbol{I} = \boldsymbol{U}_V \boldsymbol{\Lambda} \boldsymbol{U}_V^{\mathrm{H}} \tag{29}$$

where $\boldsymbol{a}_v$ denotes the velocity phase vector, defined as $\boldsymbol{a}_{v,n}(\theta_{f_d}) = \mathrm{e}^{\mathrm{j}2\pi n \theta_{f_d}}$. And $\boldsymbol{U}_V = [\boldsymbol{U}_v \boldsymbol{U}_{\mathrm{noise}}]$ is an N-dim eigenvector matrix whose first column vectors relate to the velocity estimation subspace by $\boldsymbol{U}_v$. In the same way, we obtain velocity estimation from the peak phase, given by

$$P(\theta_{f_d}) = \frac{1}{\boldsymbol{a}^{\mathrm{H}}(\theta_{f_d}) \boldsymbol{U}_{\mathrm{noise}} \boldsymbol{U}_{\mathrm{noise}}^{\mathrm{H}} \boldsymbol{a}(\theta_{f_d})} \tag{30}$$

V. Experimental Evaluation

The proposed approach enables the realization of ISAC system based on conventional C-V2X devices with limited modification. Simulations are carried out to test the performance of the proposed ISAC system based on C-V2X, with both sensing accuracy and communication throughput considered.

The C-V2X network mainly focuses on NR-V2X, with center frequency both in FR1 and in FR2 considered. In sub-6G band, center frequency is assumed as $f_c = 3.5$ GHz and $f_c = 50$ GHz in mmWave band. The main downlink physical channels and signals are modeled in NR Uu and sidelink, as is described in Section II. In the evaluations, the ISAC waveform is set with carrier bandwidth 50 MHz. The different SCS 30 kHz/60 kHz/120 kHz and nCP/eCP waveforms based on NR-V2X waveform are considered. Same as the downlink trans-

mit radio frame of 10 ms in NR, timeslots are assumed as 20 with different duration depending on different SCS.

We evaluate the feasibility of MUSIC-based sensing function for high-precision range/velocity estimation, comparing to the periodogram-based OFDM radar. The resolution of range and velocity can be derived from (23) and (24),

$$\Delta r = \frac{c}{2M\Delta f},\ \Delta v = \frac{c}{2NTf_c} \tag{31}$$

For a given SCS Δf and symbol duration T, the maximum round-trip delay $\tau_{\max}$ and Doppler shift $f_{d\max}$ need to satisfy

$$\tau_{\max} < T,\ f_{d\max} < \Delta f \tag{32}$$

Because the maximum delay is limited by symbol duration, with particular by CP duration. Therefore, the maximum range is yielded as

$$R_{\max} < \frac{c\tau_{\max}}{2} < \frac{cT_{\mathrm{CP}}}{2} \tag{33}$$

and to avoid interchannel interference (ICI), the maximum Doppler shift needs be significantly smaller than the SCS. So the maximum velocity is

$$V_{\max} \ll \frac{cf_{d\max}}{2f_c} \tag{34}$$

To satisfy the system, we set the overall feasible space contains range up to a one-way delay of half duration of CP, and velocity up to a Doppler shift of ±10% of SCS. With the above waveform numerologies, the main sensing performance parameters are summarized in Table 1.

Table 1 Sensing performance analysis

Waveform	Parameter	1	2	3	4
Configuration	Δf (kHz)	30	60	60	120
	CP	Normal	Normal	Extended	Normal
	T_{CP} (μs)	2.34	1.17	4.17	0.59
	N_{RB}	133	65	65	32
	Slot symbol	14	14	12	14
	M	1596	780	780	384
	N	280	280	240	280
	T_s (μs)	33.33	16.67	16.67	8.33
	T (μs)	35.67	17.84	20.84	8.92
	f_c (GHz)	3.5	3.5	3.5	50
System performance	Δr (m)	3.133	3.205	3.205	3.255
	Δv (m/s)	4.2911	8.5797	8.5687	1.2862
	$R_{\max}$ (m)	351	175.5	625.5	88.5
	$V_{\max}$ (m/s)	±128.57	±257.14	±257.14	±36.00

We simulate the ISAC system based on C-V2X for a single-target vehicular scenario, as discussed in Section III. We choose the distance and the relative speed between the target vehicle and RSU as $R_{\max}$ and 30 m/s, which fall in the sensing feasible span. It is noted that the speed is set to such fixed value instead of $V_{\max}$ to ensure compliance with actual vehicle scenarios. The echo signal reflected by the target vehicle is received and processed by the method proposed in Section IV. After the receiver processing, the range-velocity profile is shown in left of Figure 6, where the target can be observed obviously. Specifically, the range estimation result with MUSIC-based method is given in Figure 7, comparing to periodogram-based algorithm. In this case, an NR signal is used with SCS 30 kHz and channel bandwidth 50 MHz with 133 RBs and 20 subframes. The SNR is assumed as 10 dBm. As is shown in Figure 7, the range estimation of MUSIC is 349.7579 m with error of ~0.18%, while that is estimated as 375.7181 m with error of ~7.04% based on periodogram. We also obtain the velocity estimation result of MUSIC-based and periodogram-based method, as is shown in Figure 8. It can be seen that the velocity es-

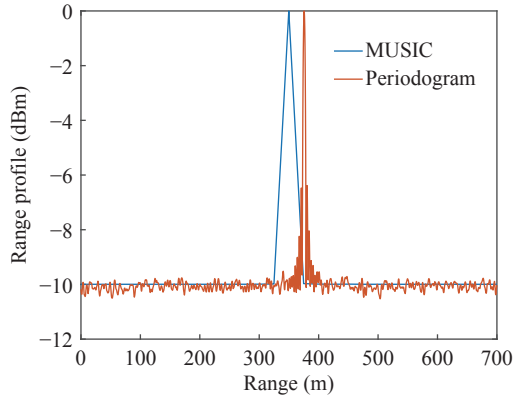

Figure 7 Range estimation with two different methods.

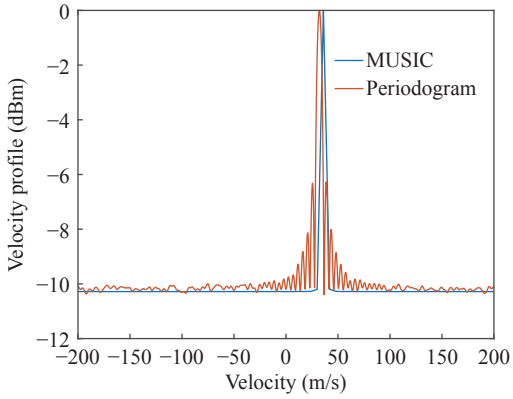

Figure 8 Velocity estimation with two different methods.

timation of MUSIC is 30.2504 m/s with error of ~0.83% and 32.1665 m/s with error of ~7.22% by periodogram, respectively. That proves the advantage of MUSIC-based method in ISAC system for V2X scenario, which satisfies high accuracy sensing with errors below 1 m and 1 m/s.

We evaluate the detection performance for varying SNR with different SCS and timeslots, as is shown in Figure 9. In these cases, we choose the fixed 50 MHz channel bandwidth and similar waveform configuration. It indicates that the probability of target detection grows with increasing SNR. Reliable target detection can be achieved up to SNR of 10 dBm, and when SNR down to −20 dBm, it nearly cannot provide successful detection. It shows a rapid plummet between the threshold, the exact number depending on SCSs and timeslots. With fixed channel bandwidth, SCS corresponds to the number of subcarrier. As it can be seen, the larger number of subcarriers and timeslots, the better detection performance can be obtained at low SNR. This is owing to the processing gain provided by cumulation of subcarriers and timeslots. In general, as discussed in [37], it obeys $G_p = k10\log(MN)$.

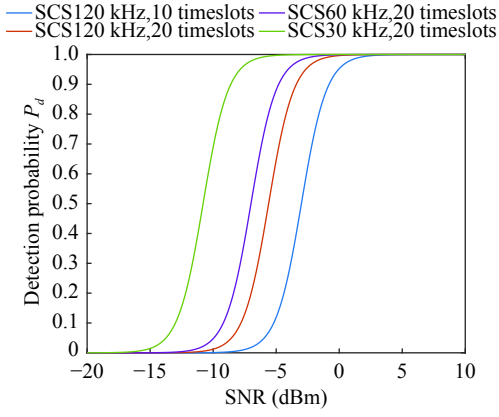

Figure 9 Detection probability with different SNR.

Further, Figures 10 and 11 present the range and velocity estimation root MSE (RMSE) behavior, respectively. The parameters configuration is similar with the waveform used above detection performance analysis, with only 20 timeslots considered. Different SCS and nCP/eCP is analyzed under similar channel bandwidth in sub-6G (3.5 GHz) and mmWave (50 GHz) band. The results prove that at those SNR with high detection probability, the range and velocity estimation RMSE are well-behaving, which is similar to the trend of detection performance. Especially, focusing on Figure 10, the inflection point where the range estimation performance degrades corresponds to threshold of P_d. When P_d is approaching 100%, the estimation RMSE is converging to a stable value. Additionally, such exact value is < 1.5 m with MUSIC-based method firmly better than the range estimation with periodogram-based method under well receiver SNR. The similar results are shown in Figure 11. The estimation RMSE values are mainly related to the velocity resolution defined in (36), which is inversely proportional to symbol duration. With the result of range and velocity estimation considered comprehensively, the best performance is obtained in SCS 30 kHz with nCP. This corresponds to the resolution value calculated in Table 1.

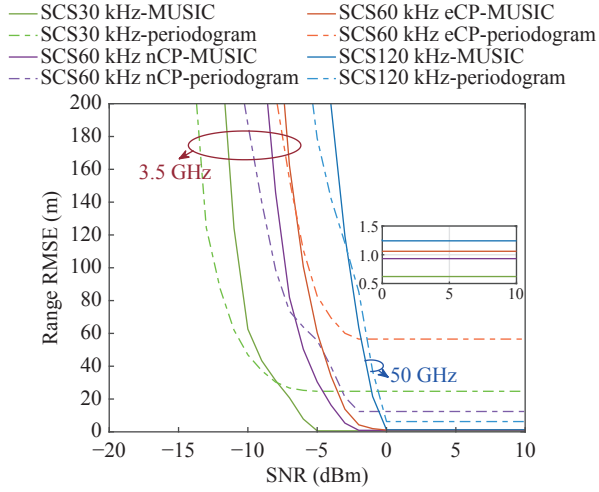

Figure 10 Range estimation RMSE with different SCS and CP.

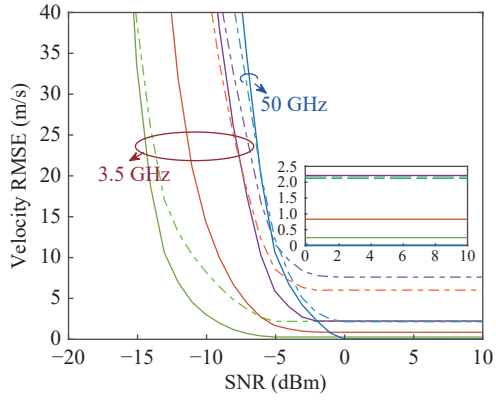

Figure 11 Velocity estimation RMSE with different SCS and CP.

To evaluate the communication performance of proposed ISAC system for C-V2X, we investigate the throughput under different SNR. As described in Section III, we simulate the communication link in vehicu-

lar scenario. With CDL-C propagation channel modeled between RSU and vehicle, the processing chain uses a single bandwidth part across the whole carrier and HARQ operation with 16 processes. The number of Tx antennas (RSU side) and Rx antennas (target vehicle side) is 8 and 2, respectively. Displaying the measured throughput in 2 frames, the percentage of the maximum possible throughput of links is shown in Figure 12. We also calculate the throughput rate with given available resources for data transmission, as is presented in Figure 13. It is obviously seen that well-behaving communication performance can be obtained under high SNR. Specifically, high reliability communication can be realized with 99.9999% and high throughput rate can be achieved with 160 Mbps if proper combination of SCS and timeslots is selected in ISAC system.

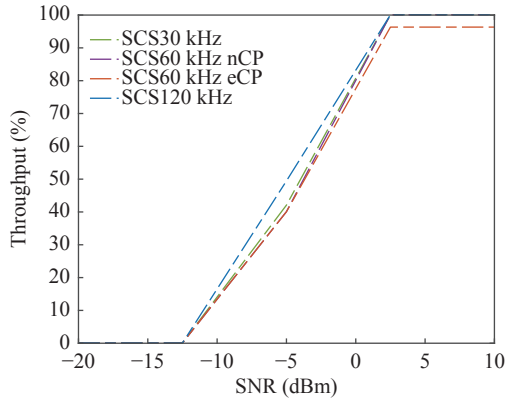

Figure 12 Percentage of maximum communication throughput.

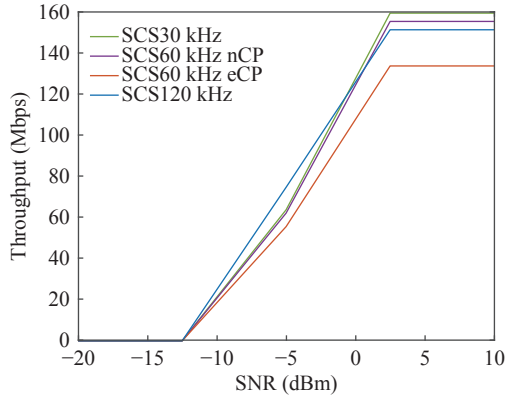

Figure 13 Throughput rate of communication link.

Both communication and sensing achieve the best performance in high SNR. This causes the tradeoff between communication and sensing when the power is allocated in ISAC system. Specifically, as is shown in Figure 9, the sensing detection probability is affected by sensing signal receiver SNR. A similar conclusion can also be made about the communication throughput from Figure 13. Therefore, the performance is positively correlated with SNR for both communication and sensing tasks. On the one hand, if the communication and sensing tasks are realized with a single signal, the performance of the whole ISAC system will be improved with a high-power transmit signal. On the other hand, if the two tasks are carried on different communication subcarriers, the power of transmit signal will be allocated between communication and sensing. This can introduce a trade-off between two tasks.

VI. Conclusion

In this paper, we developed an ISAC system based on the C-V2X standard to enable communication and sensing tasks in vehicular network. First, the performance limitation of NR waveform for sensing was analyzed by ambiguity function. Then, we formulated the model of the designed ISAC system based on NR-V2X. Receiver processing algorithm was investigated for such C-V2X-based ISAC system to achieve ultra reliability for vehicle communication and high accuracy for environment sensing. We evaluated the performance of proposed algorithm by both theory and simulations analytically. The target vehicle can be detected very reliably at high SNR. Meanwhile, the range/velocity estimation of the target can achieve with low error and high resolution. The performance of the proposed ISAC system can meet the requirement for vehicular scenarios. Additionally, the tradeoff existing between communication and sensing is analyzed because of the similar performance in high SNR. The potential applications of proposed ISAC framework will support fast vehicle platooning, secure and seamless access, and simultaneous localization and mapping.

Acknowledgements

This work was supported by the National Key Research and Development Project (Grant No. 2020YFB 1807204), the National Natural Science Foundation of China (Grant Nos. U2001213 and 61971191), the Beijing Natural Science Foundation (Grant No. L201011), the Science and Technology Foundation of Jiangxi Province (Grant No. 20202BCD42010), and the Fundamental Research Funds for the Central Universities (Grant No. 2022 YJS146).

References

[1] J. H. Zhao, X. K. Sun, Q. P. Li, *et al.*, "Edge caching and computation management for real-time internet of vehicles: an online and distributed approach," *IEEE Transactions on Intelligent Transportation Systems*, vol. 22, no. 4, pp. 2183–2197, 2021.

[2] P. Schoeder, B. Schweizer, A. Grathwohl, *et al.*, "Multitarget simulator for automotive radar sensors with unknown chirp-sequence modulation," *IEEE Microwave and Wireless Components Letters*, vol. 31, no. 9, pp. 1086–1089, 2021.

[3] J. H. Zhao, Q. P. Li, Y. Gong, *et al.*, "Computation offloading and resource allocation for cloud assisted mobile edge computing in vehicular networks," *IEEE Transactions on Vehicular Technology*, vol. 68, no. 8, pp. 7944–7956, 2019.

[4] IEEE Std 802.11™–2012, Part 11: Wireless LAN Medium Access Control (MAC) and Physical Layer (PHY) Specifica-

tion, Available at: https://standards.ieee.org/ieee/802.11, 2012.

[5] 3GPP TS 23.287, Architecture Enhancements for 5G System (5GS) to Support Vehicle-to-Everything (V2X) Services, Available at: https://www.3gpp.org/dynareport?code=23-series.htm, 2020.

[6] G. Naik, B. Choudhury, and J. M. Park, "IEEE 802.11bd & 5G NR V2X: Evolution of radio access technologies for V2X communications," *IEEE Access*, vol. 7, pp. 70169–70184, 2019.

[7] E. Grossi, M. Lops, L. Venturino, *et al.*, "Opportunistic radar in IEEE 802.11ad networks," *IEEE Transactions on Signal Processing*, vol. 66, no. 9, pp. 2441–2454, 2018.

[8] M. Bică and V. Koivunen, "Radar waveform optimization for target parameter estimation in cooperative radar-communications systems," *IEEE Transactions on Aerospace and Electronic Systems*, vol. 55, no. 5, pp. 2314–2326, 2019.

[9] R. Fu, S. Mulleti, T. Y. Huang, *et al.*, "Hardware prototype demonstration of a cognitive radar with sparse array antennas," *Electronics Letters*, vol. 56, no. 22, pp. 1210–1212, 2020.

[10] F. Liu, L. F. Zhou, C. Masouros, *et al.*, "Toward dual-functional radar-communication systems: Optimal waveform design," *IEEE Transactions on Signal Processing*, vol. 66, no. 16, pp. 4264–4279, 2018.

[11] J. H. Zhao, L. H. Yang, M. H. Xia, *et al.*, "Unified analysis of coordinated multipoint transmissions in mmwave cellular networks," *IEEE Internet of Things Journal*, vol. 9, no. 14, pp. 12166–12180, 2022.

[12] F. Liu, Y. H. Cui, C. Masouros, *et al.*, "Integrated sensing and communications: Toward dual-functional wireless networks for 6G and beyond," *IEEE Journal on Selected Areas in Communications*, vol. 40, no. 6, pp. 1728–1767, 2022.

[13] J. H. Zhao, S. J. Ni, L. H. Yang, *et al.*, "Multiband cooperation for 5G HetNets: A promising network paradigm," *IEEE Vehicular Technology Magazine*, vol. 14, no. 4, pp. 85–93, 2019.

[14] Y. Wang, Z. Q. Wei, W. Zhou, *et al.*, "Triangular FM-OFDM waveform design for integrated sensing and communication," in *2022 IEEE International Conference on Communications Workshops (ICC Workshops)*, Seoul, Korea, pp. 515–519, 2022.

[15] C. Schüpbach, C. Patry, F. Maasdorp, *et al.*, "Micro-UAV detection using DAB-based passive radar," in *2017 IEEE Radar Conference (RadarConf)*, Seattle, WA, USA, pp. 1037–1040, 2017.

[16] M. Plotka, M. Malanowski, P. Samczynski, *et al.*, "Passive bistatic radar based on VHF DVB-T signal," in *2020 IEEE International Radar Conference (RADAR)*, Washington, DC, USA, pp. 596–600, 2020.

[17] M. Ummenhofer, L. C. Lavau, D. Cristallini, *et al.*, "UAV micro-Doppler signature analysis using DVB-S based passive radar," in *2020 IEEE International Radar Conference (RADAR)*, Washington, DC, USA, pp. 1007–1012, 2020.

[18] B. Knoedler, C. Steffes, and W. Koch, "Detecting and tracking a small UAV in GSM passive radar using track-before-detect," in *2020 IEEE International Radar Conference (RADAR)*, Washington, DC, USA, pp. 1–6, 2020.

[19] W. Li, M. J. Bocus, C. Tang, *et al.*, "A taxonomy of WiFi sensing: CSI vs passive WiFi radar," in *2020 IEEE Globecom Workshops (GC Wkshps)*, Taipei, China, pp. 1–6, 2020.

[20] D. Pastina, F. Santi, F. Pieralice, *et al.*, "Passive radar imaging of ship targets with GNSS signals of opportunity," *IEEE Transactions on Geoscience and Remote Sensing*, vol. 59, no. 3, pp. 2627–2642, 2021.

[21] C. Munnell, R. Mattingly, S. Flandermeyer, *et al.*, "On the practical use and experimentation of LTE signals for radar-communications," in *2022 IEEE Radar Conference (RadarConf22)* , New York City, NY, USA, pp. 1–6, 2022.

[22] C. B. Barneto, T. Riihonen, M. Turunen, *et al.*, "Full-duplex OFDM radar with LTE and 5G NR waveforms: Challenges, solutions, and measurements," *IEEE Transactions on Microwave Theory and Techniques*, vol. 67, no. 10, pp. 4042–4054, 2019.

[23] P. Kumari, J. Choi, N. González-Prelcic, *et al.*, "IEEE 802.11ad-based radar: An approach to joint vehicular communication-radar system," *IEEE Transactions on Vehicular Technology*, vol. 67, no. 4, pp. 3012–3027, 2018.

[24] 3GPP TR 37.985, Overall Description of Radio Access Network (RAN) Aspects for Vehicle-to-Everything (V2X) Based on LTE and NR, Available at: https://www.3gpp.org/dynareport?code=37-series.htm, 2020.

[25] 3GPP TS 38.300, NR and NR-RAN Overall Description. Available at: https://www.3gpp.org/dynareport?code=38-series.htm, 2020.

[26] 3GPP TS 38.101-1, User Equipment (UE) Radio Transmission and Reception; Part 1: Range 1 Standalone, Available at: https://www.3gpp.org/dynareport?code=38-series.htm, 2020.

[27] 3GPP TR 22.886, Study on enhancement of 3GPP support for 5G V2X services, Available at: https://www.3gpp.org/dynareport?code=22-series.htm, 2018.

[28] 3GPP TS 38.211, Physical Channels and Modulation, Available at: https://www.3gpp.org/dynareport?code=38-series.htm, 2020.

[29] M. A. Richards, *Fundamentals of Radar Signal Processing*, pp. 169–170, 2005.

[30] 3GPP TR 37.885, Study on Evaluation Methodology of New Vehicle-to-Everything (V2X) Use Cases for LTE and NR, Available at: https://www.3gpp.org/dynareport?code=37-series.htm, 2020.

[31] 3GPP TR 38.321, Medium Access Control (MAC) Protocol Specification, Available at: https://www.3gpp.org/dynareport?code=38-series.htm, 2020.

[32] 3GPP TR 38.901, Study on Channel Model for Frequencies from 0.5 to 100 GHz, Available at: https://www.3gpp.org/dynareport?code=38-series.htm, 2020.

[33] 3GPP TS 38.213, Physical Layer Procedures for Control, Available at: https://www.3gpp.org/dynareport?code=38-series.htm, 2020.

[34] 3GPP TS 38.214, Physical Layer Procedures for Data, Available at: https://www.3gpp.org/dynareport?code=38-series.htm, 2020.

[35] M. Braun, C. Sturm, and F. K. Jondral, "Maximum likelihood speed and distance estimation for OFDM radar," in *2010 IEEE Radar Conference*, Arlington, VA, USA, pp. 256–261, 2010.

[36] A. M. Elbir, "DeepMUSIC: multiple signal classification via deep learning," *IEEE Sensors Letters*, vol. 4, no. 4, article no. 7001004, 2020.

[37] C. Sturm and W. Wiesbeck, "Waveform design and signal processing aspects for fusion of wireless communications and radar sensing," *Proceedings of the IEEE*, vol. 99, no. 7, pp. 1236–1259, 2011.

Yibo LI received the B.E. degree from Beijing Jiaotong University, Beijing, China, in 2020. She is a Ph.D. candidate with the School of Electronic and Information Engineering, Beijing Jiaotong University, Beijing, China. Her research interests include vehicular communications and integrated sensing and communication.
(Email: yibolee@bjtu.edu.cn)

Junhui ZHAO received the M.S. and Ph.D. degrees from Southeast University, Nanjing, China, in 1998 and 2004, respectively. His current research interests include wireless communications and the related applications.
(Email: junhuizhao@hotmail.com)

Jieyu LIAO received the B.E. degree from Jilin University, Changchun, China, in 2018. She is a Ph.D. candidate with the School of Electronic and Information Engineering, Beijing Jiaotong University, Beijing, China. Her research interests include MIMO detection and deep learning.
(Email: 18111024@bjtu.edu.cn)

Fajin HU received the B.E. degree from East China Jiaotong University, Nanchang, China, in 2021. He is an M.S. candidate with Beijing Jiaotong University, Beijing, China. His current research interest focuses on wireless communication resource management.
(Email: 21120064@bjtu.edu.cn)